Applied Thermal Engineering 78 (2015) 196–208

Contents lists available at ScienceDirect

Applied Thermal Engineering

journal homepage: www.elsevier.com/locate/apthermeng

Research paper

A novel hybrid design algorithm for spiral coil energy piles that considers groundwater advection

Gyu-Hyun Go [a], Seung-Rae Lee [a,*], Han-Byul Kang [b], Seok Yoon [a], Min-Jun Kim [a]

[a] Department of Civil and Environmental Engineering, KAIST, Daejeon, 305-701, Republic of Korea
[b] Underground Space R&D Team, R&D Division, Hyundai E&C, Yongin, 446-912, Republic of Korea

HIGHLIGHTS

- New design algorithm for spiral coil energy piles is proposed.
- Effect of groundwater advection on the design length of heat exchangers is investigated.
- Heat advection due to the groundwater flow can considerably influence the thermal interference effect.
- Hybrid GSHPs design can provide suitable alternatives that reduce the total heat exchanger length.

ARTICLE INFO

Article history:
Received 4 November 2014
Accepted 23 December 2014
Available online 30 December 2014

Keywords:
Hybrid GSHP system
Groundwater advection
Numerical analysis
Energy pile
Spiral coil heat exchanger

ABSTRACT

This paper presents a novel hybrid design algorithm for spiral coil energy piles that considers groundwater advection. The design algorithm considers the groundwater advection effect using an analytical model. During this study, the accuracy of the analytical model was verified for its design application using a finite element (FE) numerical model, and the effect of groundwater advection on the design results was investigated. According to these results, groundwater advection attenuates thermal interference between piles, as well as long-term ground thermal resistance, which contributes to the economical design of energy piles. Moreover, when there is an extreme disparity between cooling and heating loads, hybrid design was achieved using hourly building energy load data calculated by the design builder program. Hybrid design decreases the total heat exchanger length of the energy piles, and reduces the entering water temperature (EWT) variance caused by heat interference. Furthermore, the pile arrangement can influence the impact caused by separation distance. For a square arrangement of piles, the shorter the separation distance, the less the effect from the hybrid system. In contrast, for a linear arrangement of piles, there is no influence caused by the separation distance, and generally, a high reduction rate of heat exchanger length is shown.

1. Introduction

Along with recent rises in fuel costs and global warming problems, it has become a growing interest in alternative energy sources that are renewable and pollute less. In particular, Ground Source Heat Pump (GSHP) systems have become very attractive for space cooling and heating in residential and commercial buildings owing to their high efficiency and reliable operation [1–9]. These systems use the relatively uniform temperature underground as a heat reservoir: it is a source for heating in winter, and a sink for cooling in summer. Though there are various types of GSHP systems, the closed loop system using vertical-borehole ground heat exchangers is the most common type. However, the high initial installation cost of drilling the boreholes, is drawing attention to the use of foundation piles of buildings for heat exchange (called energy piles) [10–13]. This innovative idea has led to notable progress in the use of GSHP systems by making them more sustainable and by reducing their spatial requirements [14]. Compared to conventional vertical boreholes, energy piles are shorter and of larger diameter (Fig. 1). In general, energy piles less than 30 m deep are most widely used in Korea because bedrock is shallow there. Owing to its shortness, the energy pile requires a novel heat exchange pipe configuration (e.g., spiral coil heat exchanger). This type, compared with serial or parallel U-tubes, has the advantage of a greater heat transfer area

* Corresponding author. Tel.: +82 42 350 3617; fax: +82 42 350 7200.
E-mail address: srlee@kaist.ac.kr (S.-R. Lee).

http://dx.doi.org/10.1016/j.applthermaleng.2014.12.060

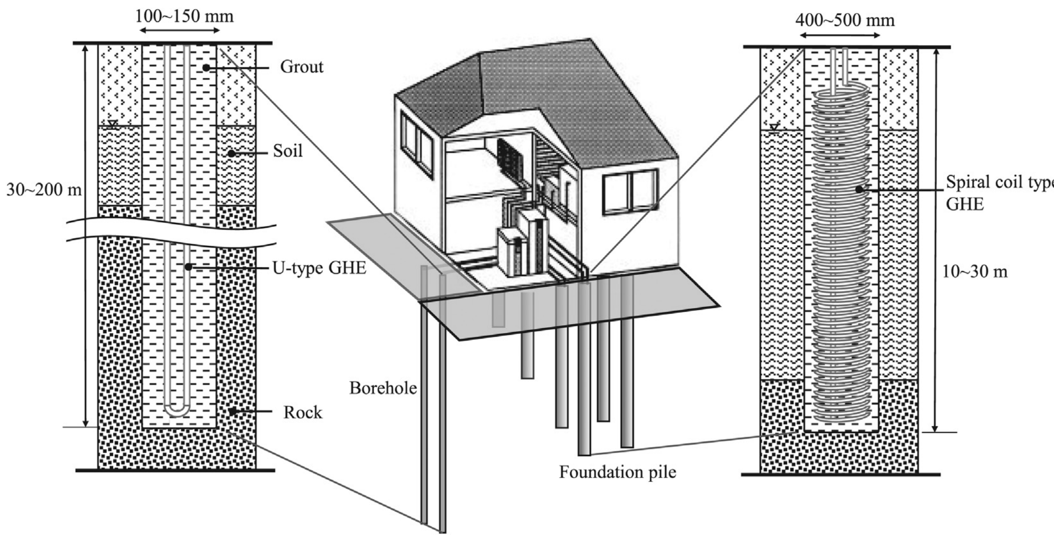

Fig. 1. Schematic diagram of vertical borehole and energy pile [22].

and a better flow pattern that eliminates air-choking in the pipes [15].

For these reasons, a number of studies have been conducted to investigate the thermal behavior of spiral coil energy piles [13,16–23]. Cui et al. [13] developed the ring coil heat source model to investigate transient heat transfer around spiral coil energy piles. They evaluated and discussed the influence of the coil pitch and locations on specific solutions. Zhang et al. [16] illustrated existing heat transfer models, and considered the ring coil model as the most realistic standard, based on heat transfer analysis of spiral coil energy piles. More recently, Zhang et al. [17] developed a new mathematical model for describing the heat transfer of energy pile considering groundwater seepage effects. Man et al. [18] developed a spiral heat source model, which provides a desirable tool for simulating a spiral coil heat exchanger, which is advantageous in dealing with short-term temperature response. Park et al. [19] suggested an efficient spiral coil source model that considered the effects of three-dimensional shape, and the radial dimension effect, using Green's function. The model used an error function to improve and simplify computation for engineering applications. Li and Lai [20] presented a continuous cylindrical surface model (which could consider composite media) for a spiral coil heat exchanger. Zarrella et al. [21] conducted a comparative study of spiral coil and triple U-tube configurations inside a foundation pile using field tests and numerical analysis. The results showed that the spiral coil energy pile provided better thermal performance than the triple U-tube configuration; there was an increase of about 23% at peak. Go et al. [22] suggested a multiple regression equation for estimating the effective borehole thermal resistance of spiral coil energy piles, and verified its accuracy via a field thermal response test (TRT) test. Park et al. [23] examined the relative constructability and thermal performance of coil type heat exchange pipes in cast-in-place concrete piles using thermal response and thermal performance tests.

Meanwhile, GSHP systems, including those with energy piles, sometimes face challenges. When there is extreme disparity between the heating and cooling loads, the change of ground temperature in the region of the GSHP system becomes more severe over time. This undesirable effect could be moderated by increasing the length of the heat exchangers, but the higher cost might be unacceptable. Another alternative would be to add an additional heat sink or source [24]. Especially in cooling dominated areas, GSHP systems could be combined with auxiliary heat rejection systems to avoid load imbalance, producing what is called a hybrid GSHP system [25,26]. Though cooling towers are the most common heat sink devices, solar power generating systems and solar water heating systems could also be used to reduce summer cooling loads.

In hybrid GSHP systems, the optimum capacity and control strategy of the supplementary equipment can be important factors, considering their long-term operation. Yavuzturg and Spitler [26] compared several control strategies for hybrid GSHP systems. Thornton [27] performed an analysis of a hybrid GSHP system for a building at the U.S. Navy Oceana Naval Air Station. Several researchers [28–35] have investigated the performance of hybrid GSHP systems using energy analysis or experimental analysis. Man et al. [36] considered the operation of a hybrid GSHP system with a cooling tower and studied the system using computer simulations. Man et al. [37] studied a hybrid ground coupled heat pump system for air conditioning in hot weather areas such as Hong Kong to discern the mitigation of the soil thermal imbalance problem. Ozgener [38] analyzed thermal loads of the heated solar greenhouses and investigated wind energy utilization in greenhouse heating which is modeled as a hybrid solar assisted geothermal heat pump and a small wind turbine system. Lubis et al. [24] conducted a thermodynamic analysis of a hybrid GSHP system with a cooling tower. System performance was evaluated in terms of coefficient of performance and exergy (energy efficiency). Sagia et al. [39] carried out a theoretical analysis of a cooling dominated hybrid GSHP system utilized to cover the energy demands of an office building. Fan et al. [31] conducted a theoretical analysis with TRNSYS software and elementary experimental research to determine the influence of various factors on soil heat imbalance and system operation efficiency. Klein et al. [40] suggested a hybrid heat pump system for existing buildings consisting of a retrofitted air water heat pump and a gas boiler, and examined its performance in full-year dynamic numerical simulations.

Most previous studies of hybrid GSHP systems were conducted to confirm the strengths of hybrid systems and to determine optimum operation strategies. However, little attention has been paid to study of design applications of hybrid GSHP systems for energy piles, considering realistic ground conditions. Therefore, this study proposed a novel hybrid design algorithm for spiral coil energy piles that considers groundwater advection. As shown in Fig. 2, the

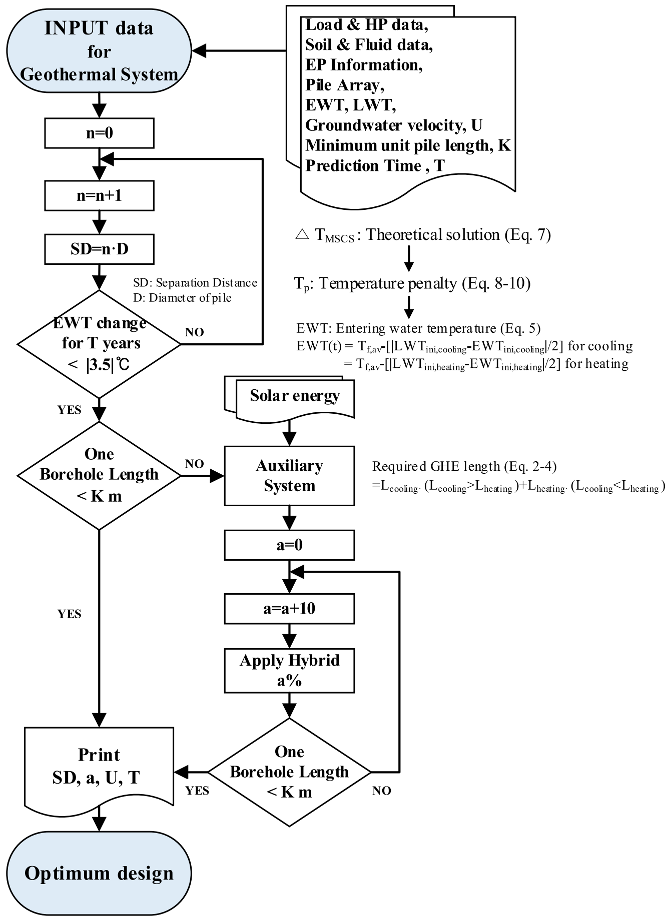

Fig. 2. Hybrid design algorithm for spiral coil energy piles that considers groundwater advection.

new design algorithm provides for optimum design by enabling the input of various parameters (i.e., building energy loads, pile array, pile length, groundwater velocity and design period). The design algorithm can consider the groundwater advection effect using an analytical model. In this study, the accuracy of the analytical model was verified for this design application using a finite element (FE) numerical model, and the effect of groundwater advection on the design results was investigated. When there was extreme disparity between the cooling and heating loads, the hybrid design process was achieved using hourly building energy load data, which were calculated by the design builder program. In this way, the best hybrid combination and optimum separation distance were provided.

2. Background theory

2.1. Design algorithm

Ingersoll et al. [41] solved a heat conduction problem in the ground, based on analytical or semi-analytical schemes, and they suggested a simple steady state heat transfer equation as shown in Eq. (1):

$$q \cdot R = L(t_g - t_w) \tag{1}$$

where q is the heat capacity (W), R is the thermal resistance, L is the required vertical length (m), t_g is the temperature at the soil interface and t_w is mean fluid temperature (K). This steady state equation can be transformed to represent the heat rate of a heat exchanger as a variable, by using a series of constant heat rate pulses. Based on this concept, Kavanaugh and Rafferty [25] proposed the heat exchanger length required for cooling and heating by considering three different heat pulses: long-term heat imbalances, average monthly heat rates during the design month, and maximum heat rates for a short-term period during the design day. The required heat exchanger length can be expressed as follows.

For cooling loads the required length is:

$$L_c = \frac{q_a R_{ga} + (q_{lc\_} W_c)\left(R_b + PLF_m R_{gm} + R_{gd} F_{sc}\right)}{T_g - T_{f,ave} - T_p} \tag{2}$$

For heating loads, the required length is:

$$L_h = \frac{q_a R_{ga} + (q_{lh\_} W_h)\left(R_b + PLF_m R_{gm} + R_{gd} F_{sc}\right)}{T_g - T_{f,ave} - T_p} \tag{3}$$

where q_a denotes the net annual average heat transfer to the ground (W), q_{lc} and q_{lh} are the building peak loads for cooling and heating (W), W_c and W_h represent the power input at design cooling and heating loads, PLF_m is the part load factor during the design month, and F_{sc} is the short circuit heat loss factor. Here, R_b is the effective borehole thermal resistance (mK W^{-1}), and the values of R_{ga}, R_{gm}, and R_{gm} represent the effective thermal resistances for three thermal pulses (mK W^{-1}): an annual pulse, a monthly pulse, and a daily pulse, respectively. Here, T_g is the undisturbed ground temperature (K), and $T_{f,av}$ represents the arithmetic mean fluid temperature (K) between inlets and outlets of the pipes. Finally, T_p represents the temperature penalty caused by thermal interference between adjacent piles; it has a positive value for heating or a negative value for cooling. The required heat-exchanger length will be the larger of the two lengths resulting from Eqs. (2) and (3).

$$\begin{aligned} Required\ \ GHE\ \ length &= L_{cooling} \cdot \left(L_{cooling} > L_{heating}\right) \\ &\quad + L_{heating} \cdot \left(L_{cooling} < L_{heating}\right) \end{aligned} \tag{4}$$

If the required heat exchanger length needed for cooling is larger than that needed for heating, the benefits of an oversized heat exchanger would be negligible during the heating season. Another alternative is to select the smaller heat exchanger length needed for heating, and then to use a hybrid system to compensate for the undersized heat exchanger. Thus, users would select the most suitable alternative considering various conditions, when designing the heat exchangers.

Once the required heat exchanger length is determined, the entering water temperature (EWT) during the design period can be calculated using back calculation of Eqs. (2) and (3). The equation for the calculation of EWT in cooling and heating modes is as follows:

$$EWT(t) = \begin{cases} T_{f,av} - \left[\left|LWT_{ini,coolling} - EWT_{ini,coolling}\right| \big/ 2\right] & for\ cooling \\ T_{f,av} - \left[\left|LWT_{ini,heating} - EWT_{ini,heating}\right| \big/ 2\right] & for\ heating \end{cases} \tag{5}$$

where $LWT_{ini,\ cooling}$ or $LWT_{ini,\ heating}$ means the water temperature leaving the heat pump at initial state for cooling and heating, respectively. Whereas, $EWT_{ini,\ cooling}$ or $EWT_{ini,\ heating}$ means the water temperature entering the heat pump at initial state for cooling and heating, respectively.

2.2. Theoretical models

There are some validated heat transfer models [13,15–20] for the spiral coil heat exchangers, which are used for estimating the ground thermal resistance such as R_{ga}, R_{gm}, and R_{gd}. Among them, the representative example is an efficient spiral coil source (SCS) model that considers three dimensional shape effects and the radial dimension effect of a spiral coil heat exchanger [19]. The solution of this model can be expressed as:

$$\begin{aligned}\Delta T_{SCS}(u,t) &= \frac{q_l}{\rho c}\int_0^t\int_0^\infty \tilde{G}(u,t;x'=r_0\cos(\omega z'),y'=r_0\sin(\omega z'),z',t')dz'dt' \\ &= \frac{q_l}{(4\pi\alpha)^{3/2}\rho c}\int_0^t \frac{1}{(t-t_0)^{3/2}}\int_0^h \exp^{\frac{F(x,y,z')}{4\alpha(t-t')}}\left(\exp^{\frac{(z-z')^2}{4\alpha(t-t')}}-\exp^{\frac{(z+z')^2}{4\alpha(t-t')}}\right)dz'\,dt' \\ &= \frac{q_l}{4\pi\lambda}\int_0^h \left[\frac{erfc\left(A_-(u,z')/2\sqrt{\alpha t}\right)}{A_-(u,z')}-\frac{erfc\left(A_+(u,z')/2\sqrt{\alpha t}\right)}{A_+(u,z')}\right]dz'\end{aligned} \tag{6}$$

with

$$F(x,y,z') = x^2+y^2+r_0^2-2xr_0\cos(wz')-2yr_0\sin(wz')$$

$$A_\pm(u,z') = \sqrt{F(x,y,z')+(z\pm z')^2}$$

where α is the thermal diffusivity ($m^2\ s^{-1}$), q_l is the heating rate per length of pile ($W\ m^{-1}$), ρ is the density ($kg\ m^{-3}$), c is the specific heat ($J\ kg^{-1}\ K^{-1}$), $\omega = 2N\pi/h$ means the wave number, and $erf(\xi) = \frac{2}{\pi}\int_0^\xi e^{-u^2}du$ denotes the error function.

Meanwhile, ground conditions such as groundwater advection, can influence both temperature penalty and ground thermal resistance. Ultimately, ground conditions can affect the design length of the heat exchangers. For this reason, combined heat transfer models that can consider conduction and advection together, have been proposed for use with these analytical approaches. Sutton et al. [42] and Diao et al. [43] proposed the moving infinite line source (MILS) model and Nelson et al. [44] evolved this model with Green's function to consider the axial effects of heat exchangers. More recently, Kang [45] suggested the moving spiral coil source (MSCS) model in order to represent the groundwater advection effect by inserting an additional term into the spiral coil source (SCS) model (Eq. (6)). Thus, the MSCS model can be expressed as:

$$\begin{aligned}\Delta T_{MSCS}(u,\tau) &= \frac{q_l}{\rho c}\int_0^t\int_0^h \tilde{G}\left(u,t;x'=r_0\cos(\omega z'),y'=r_0\sin(\omega z'),z',t'\right)dz'dt' \\ &= \frac{q_l}{(4\pi\alpha)^{3/2}\rho c}\int_0^t \frac{1}{(t-t')^{3/2}}\int_0^h e^{-\frac{F(x-U\cdot(t-t'),y,z')}{4\alpha(t-t')}}\left(e^{-\frac{(z-z')^2}{4\alpha(t-t')}}-e^{-\frac{(z+z')^2}{4\alpha(t-t')}}\right)dz'dt'\end{aligned} \tag{7}$$

where $U = u_x\cdot\rho_w\cdot c_w/\rho c$ indicates the revised velocity and u_x denotes the uniform Darcy velocity in x-direction (m/s).

2.3. Effect of thermal interference

In nearly all cases of geothermal system design, ground heat exchangers are not installed singly. A thermal interference effect is generated between piles; therefore, the efficiency of geothermal systems can either improve or deteriorate depending on the number of piles and the intervals between them. Fig. 3(a) presents an example of a 3 x 3 pile arrangement. Due to the piles at the top and bottom, and to the left and right, the heat emitted or absorbed by surrounding eight piles to the center pile in the diagram, is blocked or insufficiently absorbed. Kavanaugh and Rafferty [25] calculated the thermal storage accumulated between piles and reflected the thermal interference effect. The variable T_p in Eqs. (2) and (3), was used to take into consideration the thermal interference effect. The average "temperature penalty" T_p within the area in which the piles are arranged, is a correction factor that reflects the average temperature change in the ground. For example, when the cooling load is greater than the heating load (of the annual load), heat accumulates in the ground and the ground temperature rises because of prolonged operation, thus gradually decreasing the cooling efficiency and gradually increasing the heating efficiency. In this case, T_p has a negative value and makes corrections so that the depth of the heat exchanger required for cooling is increased. In contrast, the depth required for heating is decreased. When the heating load is greater, in which T_p has a positive value. Fig. 3(b) shows the thermal storage, which accumulates in a cylindrical form between the piles. The thermal storage of each cylinder can be calculated by multiplying the mass and specific heat of the cylinder, and the temperature change at the center points in the cylinder. For this temperature change term, a different analytical model can be used according to the type of ground heat exchanger. The stored heat that accumulates in each cylindrical space is given in Eq. (8).

$$Q_{stored} = \rho c L \pi \left[(r_o)^2 - (r_i)^2 \right] \Delta t \tag{8}$$

where L represents the required depth of the ground heat exchanger when T_p is -1.7 °C, r_o and r_i represent the outer diameter and inner diameter of the cylinder, respectively, and Δt represents the temperature change according to the analytic model. The initial T_p value is the initial estimate hypothesized by Kavanaugh. Using L calculated in this way, the final required depth can be obtained once again. As with the center piles in Fig. 3(b), for temperature change when disparate piles are located in all four directions (east, west, north, and south); the following equation is used.

$$T_{p1} = \frac{Q_{stored}}{\rho c (d_{sep})^2 L} \tag{9}$$

where d_{sep} represents the interval between the centers of the piles. In an actual design, however, when piles are located in the corners or in a straight line, instead of there being disparate piles in all four directions, a pile may be adjacent to three, two, or one pile. Partial factor, PF, is used to reflect this, and the final T_p can be calculated as follows:

$$PF = \frac{N_4 + N_3 + N_2 + N_1}{Total\ number\ of\ piles} \qquad T_p = PF \cdot T_{p1} \tag{10}$$

where, N_4, N_3, N_2, or N_1 represents the number of piles surrounded by four, three, two, and one pile, respectively. For example, as shown in Fig. 3, in the case of piles in a 3 × 3 arrangement, N_4 is 1, N_3 and N_2 are 4, and PF is 0.444. The average temperature increase or decrease T_p of the ground base surrounding the piles, is obtained by multiplying T_{p1} and PF. As that has been shown above, even in calculations of T_p, the diverse analytical solutions mentioned in Section 2.2 are used. In particular, because heat advection due to the groundwater flow can considerably influence the thermal interference effect, the use of accurate analytical solutions is necessary.

2.4. Conceptual design of hybrid system

In general, when considering load characteristics of office buildings, cooling loads tend to be dominant due to the high heat generation by office equipment such as computers. However, if the cooling dominated loads last a long time, the performance of the GSHP system will gradually decrease, and the heat pump will be damaged in the end. For this reason, guidelines for renewable energy facilities in Korea [46] clearly state that the EWT variance should not exceed the limit (±3.5 °C). Hybrid GSHP designs, coupling conventional GSHP systems with supplemental heat rejection or extraction systems, can provide suitable alternatives that reduce the EWT variance and total heat exchanger length if the load imbalance is severe. For example, though the cooling loads are most concentrated during summer months, the sun will also reach its highest point at the same period (Fig. 4). This time is favorable for obtaining the solar energy to increase efficiency. Then the solar power generating systems and solar water heating systems based on thermo-siphons or geyser pumps could be utilized to reduce summer cooling requirements. In the hybrid GSHP system, knowing when the hybrid system is predicted to be on and off hour-by-hour, enables the designer to accurately predict peak and total energy loads and to properly design the heat exchanger for target EWTs. This finally leads to more stable ground temperatures, and to

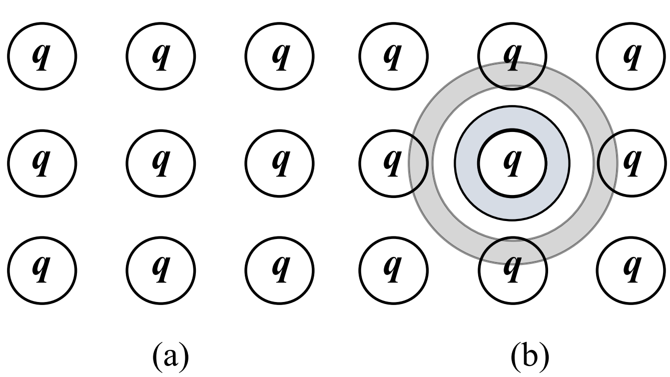

Fig. 3. Group energy pile arrangement: (a) 3 × 3 pile arrangement, and (b) thermal storage accumulated by thermal interference between piles.

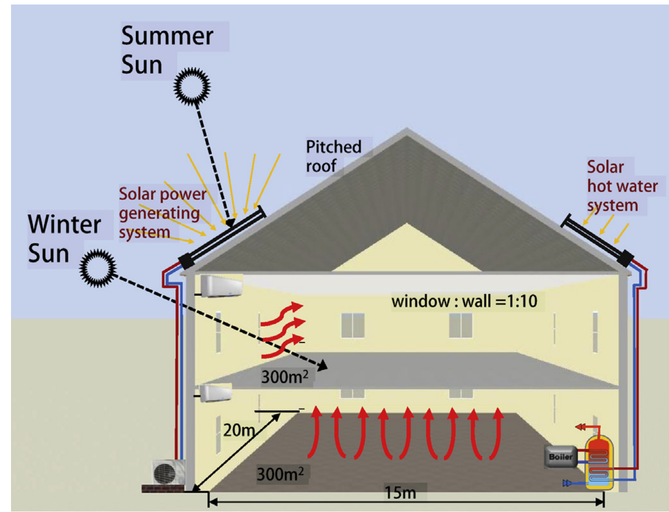

Fig. 4. Conceptual scheme of hybrid GSHP system for excess cooling loads.

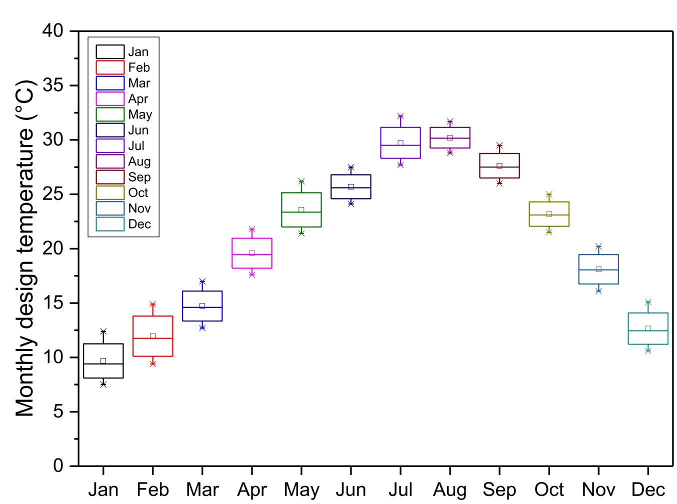

Fig. 5. Monthly design temperature distribution in Yeosu area.

Table 1
Detailed information about the Yeosu area.

Country	Republic of Korea
Source	[a]ASHRAE/[b]IWEC
Climate region	4A
Koppen classification	Cfa
Latitude	34.73
Longitude	127.75
Elevation (m)	67.0
Standard pressure (kPa)	100.5
Start/end of winter	Oct/Mar
Start/end of summer	Apr/Sep

[a] ASHRAE: American Society of Heating, Refrigerating and Air conditioning Engineers.
[b] IWEC: International Weather for Energy Calculations.

more efficient heat pump operation. Hence, in this study, an optimum GSHP system design algorithm was developed for spiral coil energy piles combined with an auxiliary system. Besides, the best hybrid combination (between auxiliary and GSHP systems) as well as the optimum separation distance between energy piles was determined.

3. Methodology

3.1. Method for estimating building energy loads

The aim of this study was to design a GSHP system for a two-story office building (Fig. 4). Yeosu, located in southwest South Korea, was selected as the study area. A commercial program called Design Builder [47] was used to estimate the cooling/heating energy loads of the building. Design Builder has a built-in regional climate/temperature database, which provides 53 regional climate-data sets for Korea, including Yeosu. Fig. 5 shows the monthly design temperature distribution in the Yeosu area. According to the ASHRAE handbook, the monthly information (in percentiles) is compiled to provide seasonally representative combinations of temperature, humidity, and solar conditions [48]. Other detailed information about the Yeosu area is presented in Table 1. As shown in Fig. 4, the building was 15 m wide and 20 m high, with a floor area of 300 m^2. The building had a pitched roof with a U-value of 0.16 W m^{-2} K^{-1}. Here, the U value is a measure of heat loss through a building element. The lower the U-value is, the greater resistance to heat flow and the better its insulating properties. The HVAC (heating, ventilation, and air conditioning) system installed in the building used a fan-coil unit with a COP of 1.97, and the DHW (domestic hot water) system used a type identical to the HVAC system, but its COP was 0.85. In cooling mode, the cooling set-point temperature was 24 °C and the cooling set-back temperature was 28 °C, while in heating mode, the heating set-point temperature was 22 °C and the heating set-back temperature was 12 °C. The operating times of the HVAC and DHW systems were set to 14:00–23:00 and 16:00–23:00, respectively. The lighting type was ‘suspended luminaire’, which has a general lighting template, and the lighting energy was 5 W m^{-2}–100 lux and the operation time was set at 16:00–23:00. For the activity of the office building, the occupancy density was set to 0.11 people m^{-2}. Also, the energy release from the office equipment was assumed to be 10 W m^{-2}. However, due to the characteristics of the office area, weekends and holidays were excluded from the calculation of energy loads. For the glazing template, double windows were used with a height of 1.5 m, spacing of 5 m and sill height of 0.8 m. The percentage of window to wall was assumed to be 10%. The U-value of internal glazing and external glazing was 2.166 W m^{-2} K^{-1} and 1.978 W m^{-2} K^{-1}, respectively.

3.2. Numerical analysis model

This study developed a three-dimensional finite element (FE) model using a commercial code (COMSOL Multi-Physics [49]) to

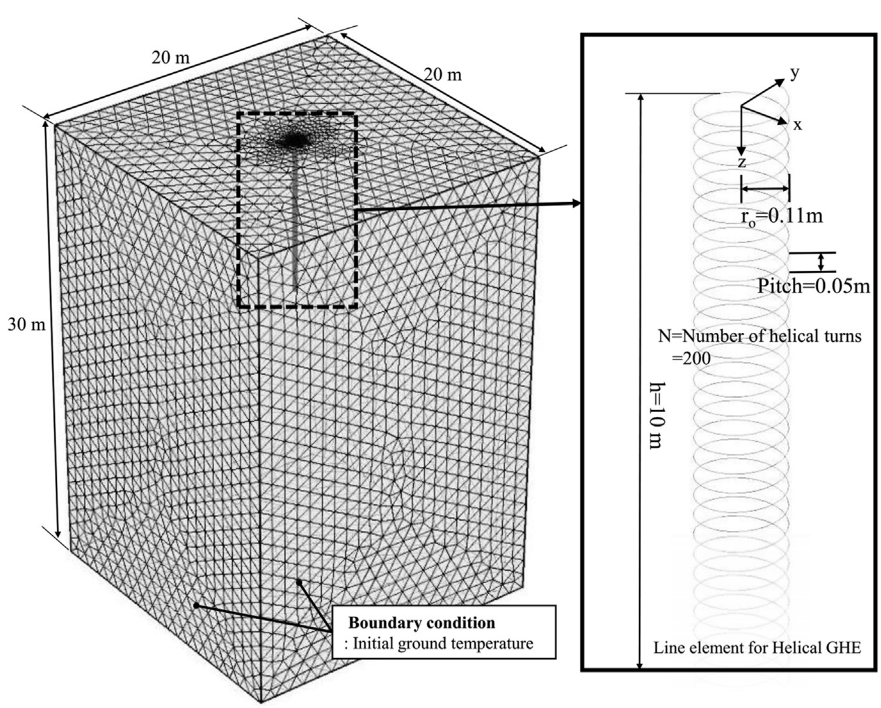

Fig. 6. Finite element model for heat transfer simulation of a spiral coil heat exchanger.

verify the accuracy of the analytical heat transfer solution, which was mentioned in Section 2.2. The major heat transfer mechanism of this model is heat conduction, but if groundwater flows inside the ground medium, the effect of advection should also be considered in the heat transfer mechanism. Hence, the domain was regarded as a porous medium, which was defined to include the three phases found in soil (solid, water and air). The governing equation of the heat transfer, based on Fourier's law, can be expressed as follows:

$$(\rho C)u\left(\frac{\partial T}{\partial x}+\frac{\partial T}{\partial y}+\frac{\partial T}{\partial z}\right)-\lambda\left(\frac{\partial^2 T}{\partial x^2}+\frac{\partial^2 T}{\partial y^2}+\frac{\partial^2 T}{\partial z^2}\right)=Q$$
$$\lambda=\sum_{i=1}^{3}\chi_i\lambda_i \quad (i = solid, water, air) \tag{11}$$

where Q means the general heat sources (W m^{-3}), ρC is the equivalent volumetric heat capacity of the porous medium (J K^{-1} m^{-3}), T is the temperature of porous medium (K), in which the local thermal equilibrium is assumed [50], and u is fluid velocity as it flows through the voids between soil particles. Also, χ_i means the volumetric fraction of each phase, and λ is the equivalent thermal conductivity of the medium (W m^{-1} K^{-1}), which can be calculated as the weighted arithmetic mean of solid, water and air. The dimensions of the FE model was 20 × 20 × 30 m (width, height, and depth, respectively; see Fig. 6). For the spiral coil heat exchanger, the coil radius is r_o, the heat exchanger depth is h, and the number of coil turns is N. The input properties are given in Table 2. With these boundary conditions, the heat transfer behavior of the spiral coil heat exchanger was predicted considering various types of groundwater flow through the ground medium.

3.3. Design information

Table 3 presents detailed information for the group energy pile design. The size of a single PHC pile was 500 mm in diameter, with thickness of 80 mm (the most commonly produced pile), and the size of the grouting material was 340 mm in diameter. Here, the thermal properties of the cement grout and the PHC pile were obtained by referring to the literature [51]. Also, the effective borehole thermal resistance was calculated using a multiple regression equation developed by Go et al. [22]. They carried out numerous parametric studies using a numerical analysis model to propose their regression model for the effective borehole thermal resistance of spiral coil energy piles. The material properties of the ground were obtained from site investigation data from the Yeosu area [52]. As shown in Fig. 7, the ground was divided into three parts: the upper part was reclamation soil, the middle part was sedimentary soil, and the bottom part was a layer of weathered granite soil. The thermal properties of each layer were taken from the literature [22,53], based on USCS. According to Yoon et al. [54], an equivalent thermal property of multi layered soils can be derived using the line source model. The ground properties presented in Table 3 were obtained from the equivalent thermal properties of multi layered soils. The heat pump was selected with a general template, which was obtained from the ground loop design (GLD) database [55]. A coiled polybutylene (PB) pipe with thermal conductivity of 0.389 W m^{-1} K^{-1} was selected, and the coil pitch was 50 mm. The circulating fluid and the groundwater were assumed to

Table 2
Input properties used for verification of the theoretical model.

Properties	Value
Heat transfer rate (W m^{-1})	20
Elapsed time (year)	1
Ground properties	
Soil thermal conductivity (W m^{-1} K^{-1})	2.30
Soil density (kg m^{-3})	2352
Soil heat capacity (J kg^{-1} K^{-1})	1061
Initial ground temperature (°C)	16
Groundwater properties	
Groundwater thermal conductivity (W m^{-1} K^{-1})	0.6
Groundwater density (kg m^{-3})	1000
Groundwater heat capacity (J kg^{-1} K^{-1})	4200

Table 3
Detailed information for the group energy pile design.

Input parameter		Value
PHC pile	Thermal conductivity (W m^{-1} K^{-1})	1.62
	Outer diameter/thickness (mm)	500/80
	Separation distance	5D–10D
Grouting	Thermal conductivity (W m^{-1} K^{-1})	2.5
	Diameter (mm)	340
Effective borehole thermal resistance (mK W^{-1})		0.108
Ground	Thermal conductivity (W m^{-1} K^{-1})	2.09
	Density (kg m^{-3})	2100
	Specific heat capacity (J kg^{-1} K^{-1})	1300
	Initial ground temperature (°C)	16
Heat pump	EER (cooling)	3.30
	COP (heating)	3.80
	EWT in cooling mode (°C)	28.0
	EWT in heating mode (°C)	8.0
	Rated flow rate (LPM)	143(cooling)/127(heating)
Pipe	Thermal conductivity (W m^{-1} K^{-1})	0.389
	Outer diameter/thickness (mm)	20/2
Coil	Diameter (mm)	0.22
	Pitch (mm)	50
Circulating fluid & groundwater flow	Thermal conductivity (W m^{-1} K^{-1})	0.57
	Density (kg m^{-3})	1000
	Specific heat capacity (J kg^{-1} K^{-1})	4200
	Groundwater velocity (m/yr)	0/2/5/10/20
Prediction time (year)		10

*D: Diameter of PHC pile.

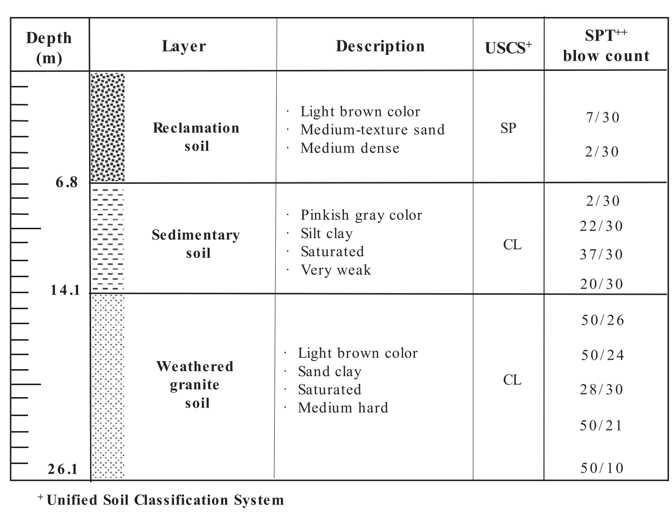

Fig. 7. Site drill log applied to the design of the GHSP system.

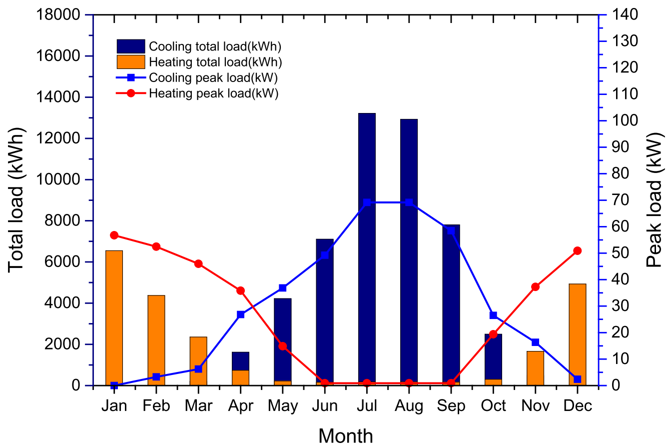

Fig. 8. Building energy load calculated by the design builder program.

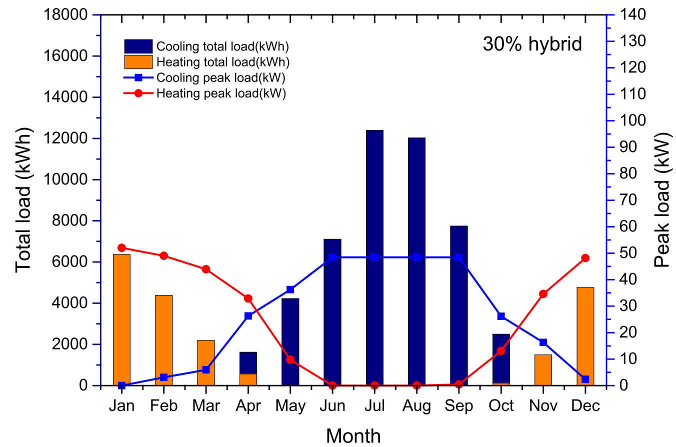

Fig. 10. Building energy load of 30% hybrid GSHP.

be pure water, and several groundwater velocities were considered (from 0 m/yr to 20 m/yr).

4. Results and discussion

4.1. Results for estimation of building energy loads

The design of the ground heat exchanger suggested by Kavanaugh and Rafffery (Section 2.1) requires building energy loads. Fig. 8 shows the cooling/heating energy loads estimated by the design builder program. Though a building demonstrated in Section 3.1 shows a passive design with a window-to-wall ratio of 10%, the cooling loads appeared to be dominant due to the load characteristics of the office building. The maximum total cooling loads and peak loads in July were approximately 1312.35 kWh and 69.17 kW, respectively. The maximum total heating loads and peak loads in January were 6548.76 kWh and 56.76 kW, respectively. The reason why the heating loads are not zero from June to September is due to the steady supply of DHW (Domestic Hot Water) used during that period. Where an extreme disparity exists between the heating and cooling loads, it is possible to reduce the glazing or increase the heat insulating capability of the wall and roof. However, it is also possible to reduce the summertime cooling loads by applying a hybrid system composed of a combination of solar

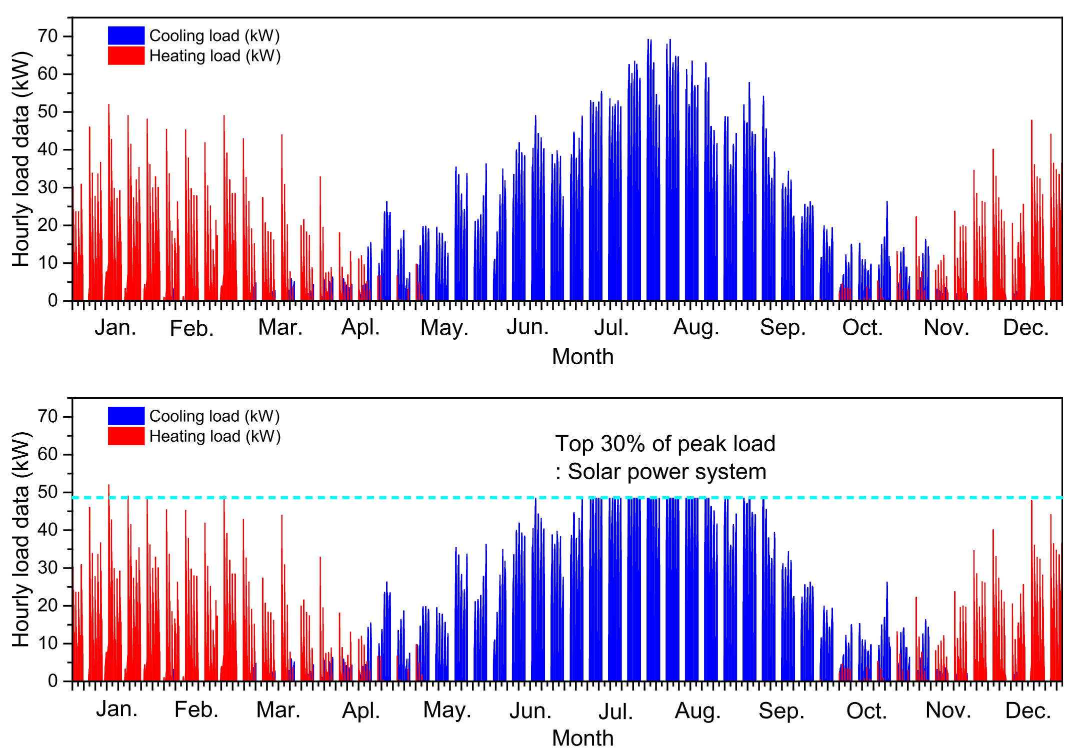

Fig. 9. Original cooling hourly loads and 30% hybrid cooling hourly loads.

Table 4
Relationship between peak and total loads in the hybrid GSHP system.

Percentage of hybrid	Peak geo loads cut	Total geo loads cut
0%	0%	0%
10%	10%	0.22%
30%	30%	3.57%
50%	50%	14.54%

power generation and solar heating water systems. In other words, using solar power systems, especially during summer, can significantly reduce the cooling load of the geothermal system. Fig. 9 shows the year-round hourly cooling/heating energy loads of the building, determined by the design builder program (excluding weekend and holiday loads). When applying a 30% hybrid system, it enabled the summertime excess cooling loads to be reduced to the 70% peak loads. These reduced cooling loads were converted to monthly total loads and monthly peak loads, and used as inputs to the hybrid geothermal energy system design (Fig. 10). When comparing the general system and the 30% hybrid system (Figs. 8 and 10), the peak loads showed a reduction from 69.17 kW to 48.42 kW, which is about a 30% reduction. Year-round total loads showed reductions from 50,117 kWh to 48,325 kWh, which is only about 3.57%. This can be confirmed by changing the ratio of the hybrid application shown in Table 4. There exists a nonlinear relationship between the hybrid ratio and the reduction percentage of the total loads. Therefore, before applying the hybrid system, one needs to check the figures of the energy loads of the building during a specified time period and compute the rate of change of the peak loads and year-round total loads. Meanwhile, Fig. 10 shows that the heating loads were reduced only slightly, and that from June to September, the heating loads equaled zero. The reasoning behind this was that the DHW relied entirely on the solar heating system during this interval.

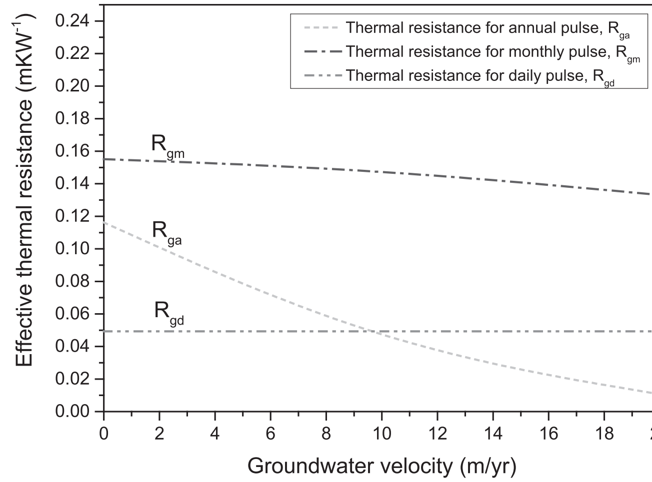

Fig. 12. Ground thermal resistance and temperature penalty according to groundwater velocity.

4.2. Effect of groundwater advection

The Kavanaugh and Rafferty design equation consists of not only the building energy loads variable, but also variables related to the ground thermal response, which are derived using the models from Section 2.2; the ground thermal response is expressed in the form of thermal resistance: R_{ga}, R_{gm}, R_{gm}. In this

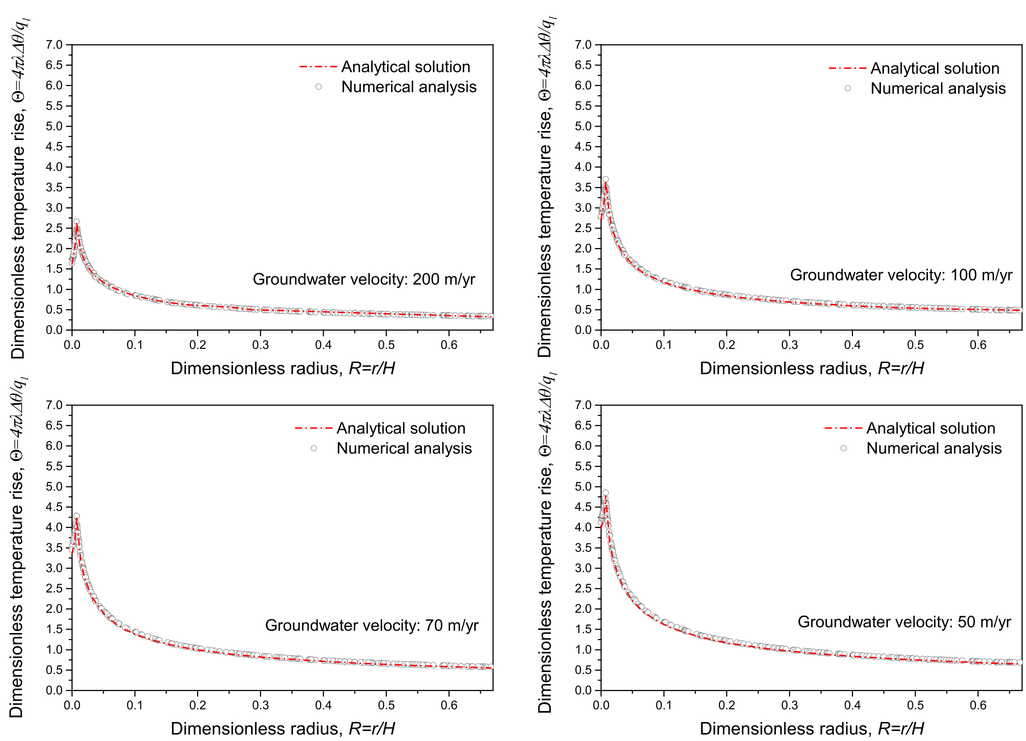

Fig. 11. Verification of analytical heat transfer model via numerical analysis.

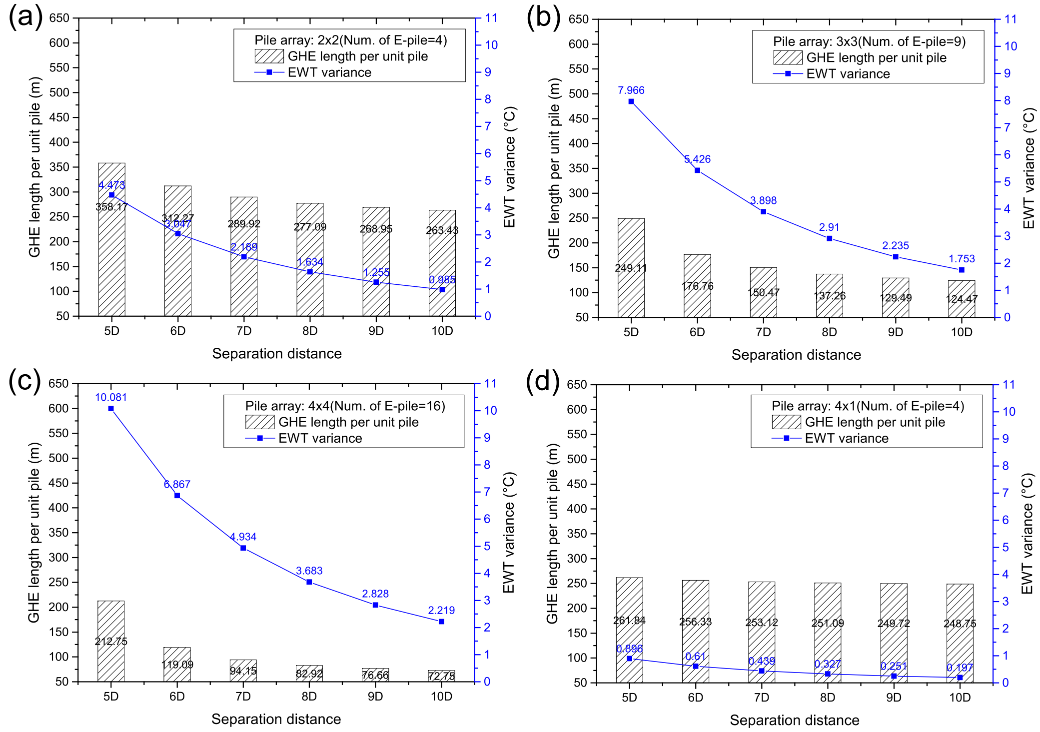

Fig. 13. Design results according to various energy pile arrays: (a) 2 × 2 pile array, (b) 3 × 3 pile array, (c) 4 × 4 pile array, and (d) 4 × 1 pile array.

study, a finite element numerical analysis program was used for the design application of the analytical models, to verify the accuracy of the model. For verification, the dimensionless variables relevant to the radial distance, and to the variation of ground temperature, were adopted. Fig. 11 shows the verification results. It can be seen that the analytical solution was in good agreement with the result of the numerical analysis, according to the major groundwater velocities. Therefore, application of an MSCS model is possible for the spiral coil heat exchanger design that considers groundwater flow. Fig. 12 shows the variance of the ground thermal resistance, which is caused by the groundwater velocity. The ground thermal resistance is affected significantly by the groundwater flow. Especially when looking at year-round thermal resistance, R_{ga} approaches zero when the flow velocity exceeds 20 m/yr. This shows that the factor of groundwater velocity may significantly influence the EWT, as well as the total length of the ground heat exchangers.

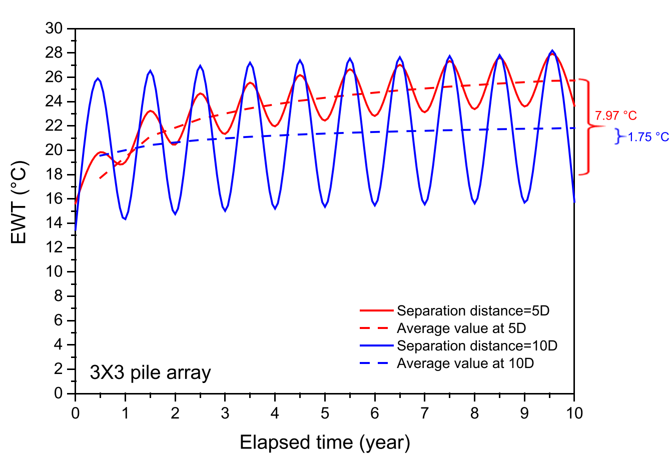

Fig. 14. EWT variation due to the thermal interference phenomenon.

4.3. Final design results

Fig. 13 plots the final design results of the energy pile for office buildings in the Yeosu area. Among these designs, the optimal design is shown to have less than 3.5 degrees of EWT variance, and to have a minimum length heat exchanger. Fig. 14 implies that the shorter the separation distance, the more the average EWT increases due to heat interference between the piles. When this phenomenon continues, it can cause a problem for operation of the heat pump. Particularly when the design has numerous piles arranged in the form of a square (Fig. 13(b) and (c)), the standard deviation of the EWT can exceed ± 3.5 °C, which is unfit for a design. However, groundwater flow can significantly reduce the variance of EWT. This is because the groundwater flow reduces the

Table 5
Temperature penalty value calculation using the MSCS Model.

Pile array	Groundwater velocity (m/yr)	Separation distance between piles					
		5D	6D	7D	8D	9D	10D
3 × 3	0	8.141	5.548	3.989	2.979	2.289	1.797
	2	5.306	3.578	2.546	1.883	1.433	1.115
	5	2.575	1.722	1.216	0.892	0.674	0.521
	10	1.397	0.933	0.658	0.483	0.365	0.282
	20	0.873	0.588	0.418	0.309	0.236	0.184
4 × 4	0	10.303	7.022	5.048	3.771	2.897	2.275
	2	6.715	4.528	3.222	2.383	1.814	1.411
	5	3.259	2.18	1.538	1.129	0.853	0.659
	10	1.769	1.181	0.833	0.611	0.462	0.357
	20	1.105	0.744	0.529	0.391	0.298	0.232

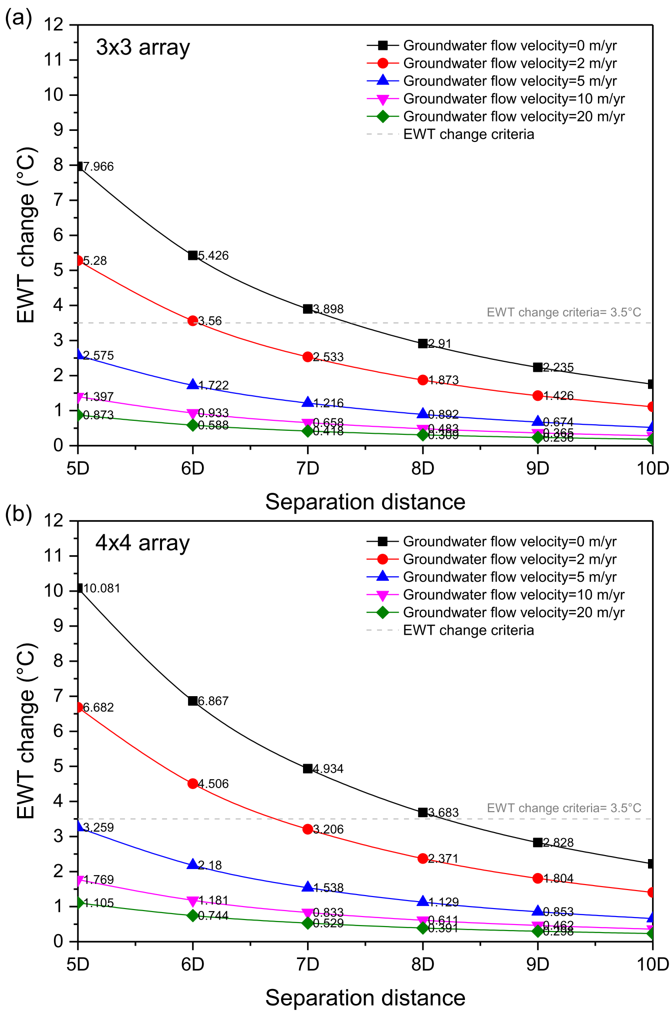

Fig. 15. Effect of groundwater advection on the EWT variance: (a) 3 × 3 pile array, and (b) 4 × 4 pile array.

heat variance of the ground. As shown in Table 5, when the groundwater velocity increases, the ground temperature penalty (T_p) decreases, and as T_p has a strong relation with EWT, the variance of EWT decreases also. Fig. 15 shows the EWT variance in relation with T_p, and the general reduction in EWT variance can be observed. If the ground has a 5 m/yr groundwater velocity, a EWT variance condition is met even in a 3 x 3 or 4 x 4 arrangement, which enables 5D distance construction. Therefore, before the construction, one can apply the groundwater flow variable in the design to improve efficiency.

Meanwhile, as shown in Fig. 13(a) and (d), when the EWT variance is moderate but the heat exchanger length is too long, the use of a hybrid system can reduce the heat exchanger length. Fig. 16 shows the heat exchanger length and EWT variance in relation to the hybrid design. When the 50% hybrid was used, the 2 × 2 pile array was reduced by up to 40% of its length, and a 4 x 1 pile array showed reduction of up to 42%. Observing the reduction of EWT variance compared to the general system, it can be inferred that the inequality problem caused by heat interference, can be solved. Furthermore, for the hybrid system (Fig. 17), the shape of the pile arrangement can influence the impact caused by separation distance. In the square arrangement, it was shown that the shorter the separation distance, the less the effect from the hybrid. This is because the heat interference from too little separation distance offsets the load attenuation effect from the hybrid system. On the other hand, in the case of the linearly arranged piles, there was no influence caused by separation, and a generally high reduction rate of heat exchanger length was shown.

5. Conclusions and summary

This study proposed a hybrid design algorithm for spiral coil energy piles that considers groundwater advection, and provided the best hybrid combination as well as the optimum pile separation distance. The design algorithm considers the groundwater advection effect using an analytical model. The study also verified the accuracy of the analytical model for its design application using the finite element (FE) numerical model, and investigated the effect of groundwater advection on the design results. Moreover, cases where extreme disparity between cooling and heating loads exists, it is possible to reduce summertime cooling loads by applying a hybrid system. The hybrid design process was achieved using hourly building energy load data, which were calculated by the Design Builder program. The main conclusions drawn from the study results can be summarized as follows:

1. Since the analytical solutions of MSCS model were in good agreement with the results of the numerical analysis, it is thought that the application of MSCS model is possible for the spiral coil heat exchanger designs that consider the groundwater flow.
2. The ground thermal resistance is affected significantly by groundwater flow. In particular, R_{ga} approaches zero when the groundwater velocity is fast. This shows that the groundwater velocity factor significantly influences the design length of heat exchangers. Moreover, owing to groundwater advection, the increase in EWT resulting from thermal interference can be considerably alleviated. In short, groundwater advection attenuates thermal interference between piles as well as long-term ground thermal resistance, which contributes to the economical design of energy piles. Therefore, in order to implement more realistic and efficient heat exchanger design, the flow characteristics of the local groundwater should be considered in advance.
3. There exists a nonlinear relationship between the hybrid ratio and the reduction percentage of the total loads. Therefore, before applying the hybrid system, one needs to check the figures on the energy loads of the building during a specified interval, and then compute the rate of change of the peak loads and year-round total loads.
4. In the final design results, the case satisfying the EWT criteria, and having the smallest possible heat exchanger length at the same time, is considered an optimum design. However, when EWT variance is moderate but the heat exchangers are too long, the heat exchanger length can be reduced intentionally using the hybrid design. Furthermore, by observing the reduction of EWT variance, compared to the general system, it can be inferred that hybrid design can solve the inequality problem, which is caused by heat interference. In addition, the pile arrangement can influence the impact caused by distance. In a square arrangement, the shorter the separation distance, the less the effect from the hybrid. On the other hand, in the case of a linear arrangement, there is no influence caused by separation distance, and generally, a high reduction rate of heat exchanger length is seen.

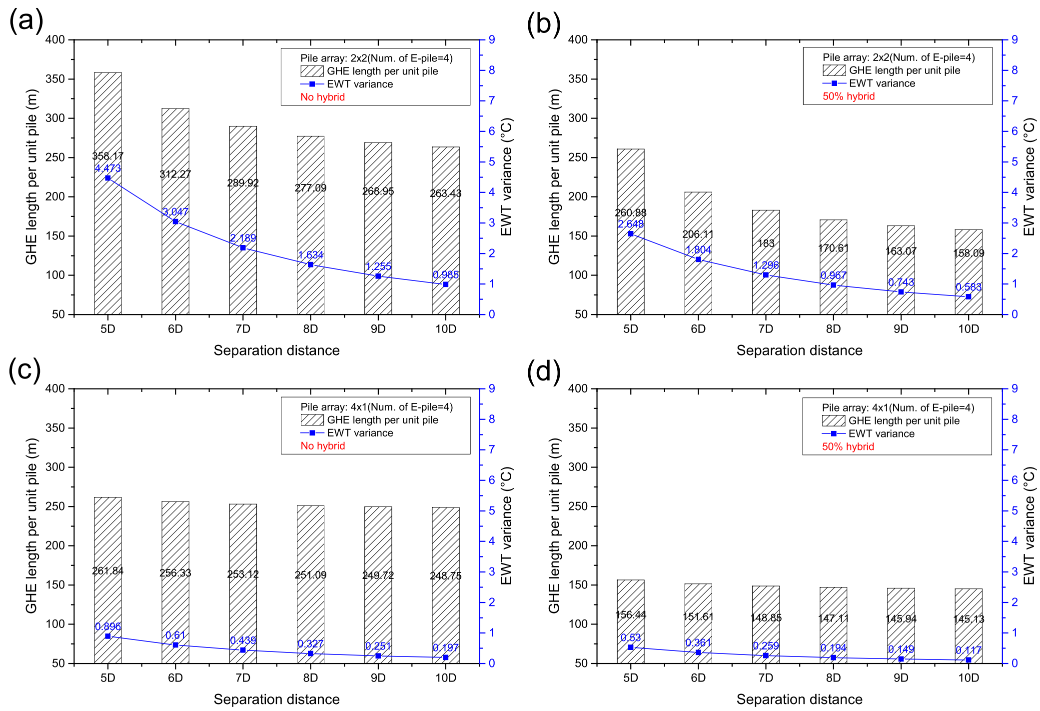

Fig. 16. Design results of hybrid GSHP system: (a) 2 × 2 pile array, no hybrid; (b) 2 x 2 pile array, 50% hybrid; (c) 4 × 1 pile array, no hybrid; and (d) 4 × 1 pile array, 50% hybrid.

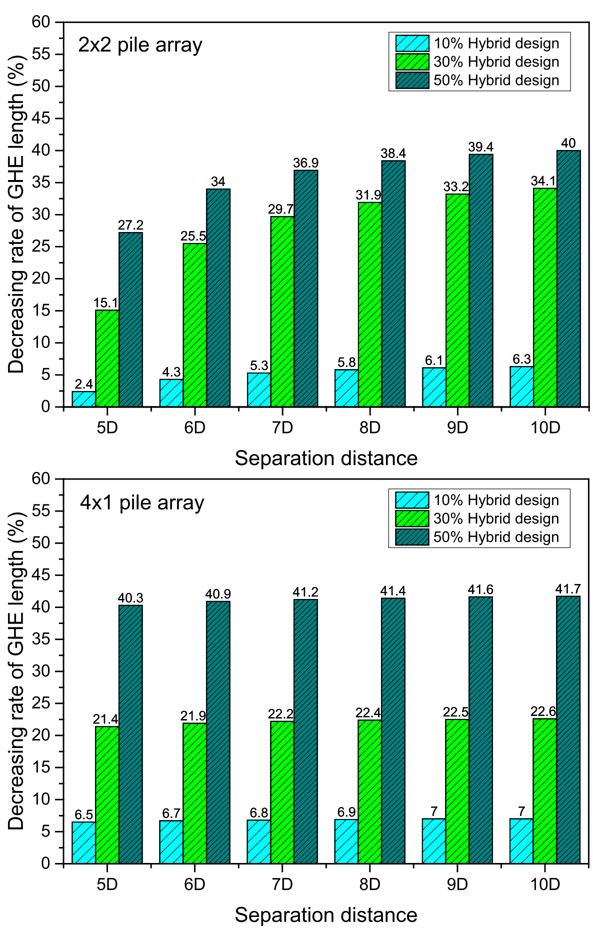

Fig. 17. Hybrid design and decreasing rate of GHE length.

Acknowledgements

This work was financially supported as a Basic Research Project of the National Research Foundation of Korea, under the Ministry of Science, ICT and Future Planning (grant No. 2013R1A2A2A01067898) and by grant 14-RDRP-B076564-01 from the Regional Development Research Program funded by the Ministry of Land, Infrastructure and Transport of the Korean government.

References

[1] International Energy Agency, Renewable Energy Essentials: Geothermal, 2010.
[2] A.M. Omer, Ground-source heat pumps systems and applications, Renew. Sustain. Energy Rev. 12 (2008) 344–371.
[3] G. Florides, S. Kalogirou, Ground heat exchangers—a review of systems, models and applications, Renew. Energy 32 (15) (2007) 2461–2478.
[4] L. Ozgener, O. Ozgener, An experimental study of the exergetic performance of an underground air tunnel system for greenhouse cooling, Renew. Energy 35 (2010) 2804–2811.
[5] O. Ozgener, L. Ozgener, D.Y. Goswami, Experimental prediction of total thermal resistance of a closed loop EAHE for greenhouse cooling system, Int. Commun. Heat Mass Transf. 38 (6) (2011) 711–716.
[6] H. Park, S.R. Lee, S. Yoon, H.S. Shin, D.S. Lee, Case study of heat transfer behavior of helical ground heat exchanger, Energy Build. 53 (2012) 137–144.
[7] H. Wang, Q. Zhao, J. Wu, B. Yang, Z. Chen, Experimental investigation on the operation performance of a direct expansion ground source heat pump system for space heating, Energy Build. 61 (2013) 349–355.
[8] O. Ozgener, L. Ozgener, Exergoeconomic analysis of an underground air tunnel system for greenhouse cooling system, Int. J. Refrig. 33 (2010) 995–1005.
[9] O. Ozgener, L. Ozgener, J. Tester, A practical approach to predict soil temperature variations for geothermal (ground) heat exchangers applications, Int. J. Heat Mass Transf. 62 (2013) 473–480.
[10] D. Pahud, A. Fromentin, M. Hubbuch, Heat exchanger pile system for heating and cooling at Zürich airport, IEA Heat Pump. Cent. Newsl. 17 (1) (1999) 15–16.
[11] L. Laloui, M. Moreni, L. Vulliet, Behavior of a dual-purpose pile as foundation and heat exchanger, Can. Geotech. J. 40 (2) (2003) 388–402.
[12] H. Brandle, Energy foundations and other thermo-active ground structures, Géotechnique 56 (2) (2006) 81–122.
[13] P. Cui, X. Li, Y. Man, Z. Fang, Heat transfer analysis of pile geothermal heat exchanger with spiral-coils, Appl. Energy 88 (2011) 4113–4119.

[14] O. Boennec, Shallow ground energy systems, Energy 161 (2008) 57–61.
[15] Y. Man, H.X. Yang, N.R. Diao, J.H. Liu, Z.H. Fang, A new model and analytical solutions for borehole and pile ground heat exchangers, Int. J. Heat Mass Transf. 53 (2010) 2593–2601.
[16] W. Zhang, H. Yang, L. Lu, Z. Fang, Investigation on heat transfer around buried coils of pile foundation heat exchangers for ground-coupled heat pump applications, Int. J. Heat Mass Transf. 55 (21–22) (2012) 6023–6031.
[17] W. Zhang, H. Yang, L. Lu, P. Cui, Z. Fang, The research on ring-coil heat transfer models of pile foundation ground heat exchangers in the case of groundwater seepage, Energy Build. 71 (2014) 115–128.
[18] Y. Man, H.X. Yang, N.R. Diao, X. Li, P. Cui, Z.H. Fang, Development of spiral heat source model for novel pile ground heat exchangers, HVAC&R Res. 17 (6) (2011) 1075–1088.
[19] S.K. Park, S.R. Lee, H.K. Park, S. Yoon, J.W. Chung, Characteristics of an analytical solution for a spiral coil type ground heat exchanger, Comput. Geotech. 49 (2013) 18–24.
[20] M. Li, A.C.K. Lai, New temperature response functions (G functions) for pile and borehole ground heat exchangers based on composite-medium line-source theory, Energy 38 (2012) 255–263.
[21] A. Zarrella, M. De Carli, A. Galgaro, Thermal performance of two types of energy foundation pile: helical pipe and triple U-tube, Appl. Therm. Eng. 61 (2013) 301–310.
[22] G.H. Go, S.R. Lee, S. Yoon, H.B. Kang, Design of spiral coil PHC energy pile considering effective borehole thermal resistance and groundwater advection effects, Appl. Energy 125 (2014) 165–178.
[23] S.W. Park, D.S. Lee, H.J. Choi, K.S. Jung, H.S. Choi, Relative constructability and thermal performance of cast-in-place concrete energy pile coil-type GHEX (ground heat exchanger), in press, Energy (2014).
[24] L.I. Lubis, M. Kanoglu, I. Dincer, M.A. Rosen, Thermodynamic analysis of a hybrid geothermal heat pump system, Geothermics 40 (2011) 233–238.
[25] S.P. Kavanaugh, K. Rafferty, Ground-source Heat Pumps: Design of Geothermal Systems for Commercial and Institutional Buildings, ASHRAE, Inc., Atlanta, USA, 1997.
[26] C. Yavuzturg, J.D. Spitler, Comparative study of operating and control strategies for hybrid ground-source heat pump systems using a short time step simulation model, ASHRAE Trans. 106 (2000) 192–209.
[27] J. Thornton, A Detailed TRNSYS Analysis of Building 137, Oceana Naval Air Station, Virginia Beach, Virginia, 2000. Project report for Oak Ridge National Laboratory.
[28] G. Phetteplace, W. Sullivan, Performance of a hybrid ground-coupled heat pump system, ASHRAE Trans. 104 (1998) 763–770.
[29] J.B. Singh, G. Foster, Advantages of using the hybrid geothermal option, in: Proceedings of the Second Stockton International Geothermal Conference, Pomona, NJ, USA, 1998.
[30] N. Pardo, Á. Montero, A. Sala, J. Martos, J.F. Urchueguía, Efficiency improvement of a ground coupled heat pump system from energy management, Appl. Therm. Eng. 31 (2011) 391–398.
[31] R. Fan, Y. Gao, L. Hua, X. Deng, J. Shi, Thermal performance and operation strategy optimization for a practical hybrid ground-source heat-pump system, Energy Build. 78 (2014) 238–247.
[32] H.S. Park, K.H. Nam, G.H. Jang, M.S. Kim, Performance investigation of heat pump–gas fired water heater hybrid system and its economic feasibility study, Energy Build. 80 (2014) 480–489.
[33] J.S. Lee, H.H. Park, Y.C. Kim, Transient performance characteristics of a hybrid ground-source heat pump in the cooling mode, Appl. Energy 123 (2014) 121–128.
[34] J.M. Choi, B. Kang, H.H. Cho, Performance comparison between R22 and R744 solar-geothermal hybrid heat pumps according to heat source conditions, Renew. Energy 71 (2014) 414–424.
[35] W. Gang, J. Wang, S. Wang, Performance analysis of hybrid ground source heat pump systems based on ANN predictive control, Appl. Energy 136 (2014) 1138–1144.
[36] Y. Man, H. Yang, Z. Fang, Study on hybrid ground-coupled heat pump systems, Energy Build. 40 (2008) 2028–2036.
[37] Y. Man, H. Yang, J. Wang, Study on hybrid ground-coupled heat pump system for air-conditioning in hot-weather areas like Hong Kong, Appl. Energy 87 (2010) 2826–2833.
[38] O. Ozgener, Use of solar assisted geothermal heat pump and small wind turbine systems for heating agricultural and residential buildings, Energy 35 (1) (2010) 262–268.
[39] Z. Sagia, C. Rakopoulos, E. Kakaras, Cooling dominated hybrid ground source heat pump system application, Appl. Energy 94 (2012) 41–47.
[40] K. Klein, K. Huchtemann, D. Muller, Numerical study on hybrid heat pump systems in existing buildings, Energy Build. 69 (2014) 193–201.
[41] L.R. Ingersoll, O.J. Zobel, A.C. Ingersoll, Heat Conduction: With Engineering and Geological Applications, McGraw-Hill, New York, 1954.
[42] M.G. Sutton, D.W. Nutter, R.J. Couvillion, A ground resistance for vertical borehole heat exchangers with groundwater flow, J. Energy Resour. Technol. ASME 125 (3) (2003) 183–189.
[43] N.R. Diao, Q.Y. Li, Z.H. Feng, Heat transfer in ground heat exchangers with groundwater advection, Int. J. Therm. Sci. 43 (12) (2004) 1203–1211.
[44] M.G. Nelson, B. Philipp, K. Zhu, P. Bayer, Z.H. Fang, A moving finite line source model to simulate borehole heat exchangers with groundwater advection, Int. J. Therm. Sci. 50 (2011) 2506–2513.
[45] H.B. Kang, Improved Design Method of Ground-source Heat Pump System and Develop Design Program, Master thesis, Korea Advanced Institute of Science and Technology, Korea, 2014.
[46] A Guideline for Support of New and Renewable Energy Equipment, New and Renewable Energy Center, Korea Energy Management Corporation, 2014.
[47] Design Builder Training Manual Ver. 5.2b, Design Builder Software Ltd, UK, 2014.
[48] International Weather for Energy Calculations (IWEC Weather Files), ASHRAE, 2001.
[49] Comsol Inc, Comsol Multiphysics User's Manual Ver. 4.3a, 2012. USA.
[50] C. Moyne, S. Didierjean, H.P. Amaral Souto, O.T. da Silveira, Thermal dispersion in porous media: one-equation model, Int. J. Heat Mass Transf. 43 (20) (2000) 3853–3867.
[51] S.S. Jeong, J.Y. Song, H.S. Min, S.J. Lee, Thermal influential factors of energy pile, J. Kor. Soc. Civ. Eng. 6 (6C) (2010) 231–239.
[52] Report of Site Investigation for Yeosu New Port, Yeosu Regional Maritime Affairs & Port Administration, Ministry of Oceans and Fisheries, 2005.
[53] H. Park, S.R. Lee, S. Yoon, J.C. Choi, Evaluation of thermal response and performance of PHC energy pile: field experiments and numerical simulation, Appl. Energy 103 (2013) 12–24.
[54] S. Yoon, S.R. Lee, G.H. Go, J. Xue, H.K. Park, D.W. Park, Thermal transfer behavior in two types of W-shape ground heat exchangers installed in multilayer soils, Geomech. Eng. 6 (1) (2014) 79–98.
[55] Adding Heat Pump Guide Ver. 5.3 through GLD 2014, Gaia Geothermal, USA, 2014.

Nomenclature

Symbol

c: specific heat (J kg^{-1} K^{-1})
F_{sc}: short-circuit heat loss factor
L: required vertical length (m)
PLF_m: part-load factor during design month
Q: general heat sources (W m^{-3})
q: heat capacity (W)
q_a: net annual average heat transfer to the ground (W)
q_{lc}: building peak load for cooling (W)
q_{lh}: building peak load for heating (W)
q_l: heating rate per length of pile (W m^{-1})
$R_{g,a}$: ground thermal resistance for annual pulse (m K W^{-1})
$R_{g,m}$: ground thermal resistance for monthly pulse (m K W^{-1})
$R_{g,d}$: ground thermal resistance for daily pulse (m K W^{-1})
R_b: borehole thermal resistance (m K W^{-1})
r_o: coil radius (m)
h: heat exchanger depth (m)
N: coil turns
$T_{f,av}$: arithmetic mean fluid temperature (K)
T_g: undisturbed ground temperature (K)
T_p: temperature penalty
T: temperature (K)
t: times (s)
t_g: temperature at the soil interface (K)
t_w: mean fluid temperature (K)
t',u': integral variable
u: vector in x, y, z Cartesian coordinates
x', y', z': integral variable

Greek letters

α: thermal diffusivity (m^2 s^{-1})
ρ: density (kg m^{-3})
ρc: equivalent volumetric heat capacity of the porous medium (J K^{-1} m^{-3})
λ: thermal conductivity (W m^{-1} K^{-1})
ω: wave number (m^{-1})

Subscripts

EWT: entering water temperature (K)
LWT: leaving water temperature (K)
SCS: spiral coil source model
MILS: moving infinite line source model
MSCS: moving spiral coil source model